Angle-dependent strong-field molecular ionization rates with tuned range-separated time-dependent density functional theory

Adonay Sissay, Paul Abanador, François Mauger, Mette Gaarde, Kenneth J. Schafer, and Kenneth Lopata

Citation: The Journal of Chemical Physics **145**, 094105 (2016); doi: 10.1063/1.4961731
View online: https://doi.org/10.1063/1.4961731
View Table of Contents: http://aip.scitation.org/toc/jcp/145/9
Published by the American Institute of Physics

Articles you may be interested in

Strong field ionization rates simulated with time-dependent configuration interaction and an absorbing potential
The Journal of Chemical Physics **140**, 174113 (2014); 10.1063/1.4874156

Real time propagation of the exact two component time-dependent density functional theory
The Journal of Chemical Physics **145**, 104107 (2016); 10.1063/1.4962422

Perspective: Fundamental aspects of time-dependent density functional theory
The Journal of Chemical Physics **144**, 220901 (2016); 10.1063/1.4953039

Dynamics of photoionization from molecular electronic wavepacket states in intense pulse laser fields: A nonadiabatic electron wavepacket study
The Journal of Chemical Physics **146**, 134114 (2017); 10.1063/1.4979672

Studies of spuriously shifting resonances in time-dependent density functional theory
The Journal of Chemical Physics **145**, 044101 (2016); 10.1063/1.4955447

Theory of attosecond delays in molecular photoionization
The Journal of Chemical Physics **146**, 124306 (2017); 10.1063/1.4977933

Angle-dependent strong-field molecular ionization rates with tuned range-separated time-dependent density functional theory

Adonay Sissay,[1] Paul Abanador,[2] François Mauger,[2] Mette Gaarde,[2] Kenneth J. Schafer,[2] and Kenneth Lopata[1,3,a)]

[1]*Department of Chemistry, Louisiana State University, Baton Rouge, Louisiana 70803, USA*
[2]*Department of Physics and Astronomy, Louisiana State University, Baton Rouge, Louisiana 70803, USA*
[3]*Center for Computation and Technology, Louisiana State University, Baton Rouge, Louisiana 70803, USA*

(Received 18 April 2016; accepted 16 August 2016; published online 2 September 2016)

Strong-field ionization and the resulting electronic dynamics are important for a range of processes such as high harmonic generation, photodamage, charge resonance enhanced ionization, and ionization-triggered charge migration. Modeling ionization dynamics in molecular systems from first-principles can be challenging due to the large spatial extent of the wavefunction which stresses the accuracy of basis sets, and the intense fields which require non-perturbative time-dependent electronic structure methods. In this paper, we develop a time-dependent density functional theory approach which uses a Gaussian-type orbital (GTO) basis set to capture strong-field ionization rates and dynamics in atoms and small molecules. This involves propagating the electronic density matrix in time with a time-dependent laser potential and a spatial non-Hermitian complex absorbing potential which is projected onto an atom-centered basis set to remove ionized charge from the simulation. For the density functional theory (DFT) functional we use a tuned range-separated functional LC-PBE*, which has the correct asymptotic $1/r$ form of the potential and a reduced delocalization error compared to traditional DFT functionals. Ionization rates are computed for hydrogen, molecular nitrogen, and iodoacetylene under various field frequencies, intensities, and polarizations (angle-dependent ionization), and the results are shown to quantitatively agree with time-dependent Schrödinger equation and strong-field approximation calculations. This tuned DFT with GTO method opens the door to predictive all-electron time-dependent density functional theory simulations of ionization and ionization-triggered dynamics in molecular systems using tuned range-separated hybrid functionals. *Published by AIP Publishing.* [http://dx.doi.org/10.1063/1.4961731]

I. INTRODUCTION

Driven by recent advances in ultrafast science, measuring electronic dynamics in molecular systems is becoming feasible on the attosecond time scale.[1–6] Probing these ultrafast dynamics promises to shed light on a range of processes including charge migration[6–9] and photochemistry,[10] with applications spanning spectroscopy[11–14] to light harvesting.[15] However, pump-probe techniques for attosecond dynamics can be challenging due to the required short intense pulses and difficulties with sample alignment. An alternate approach is to instead use time-resolved high harmonic generation (TR-HHG), where the dynamics are measured via the modulation of the harmonic spectrum generated from the rescattering of an ionized electron from the evolving parent ion.[16–18] In a three-step picture[18–20] this consists of strong-field ionization, propagation of the electronic wavepacket under the field, and scattering of the electron from the parent ion which is in a time-dependent excited state.

A first-principles description of strong-field ionization dynamics in molecules is crucial to interpreting experiments and devising new techniques for TR-HHG for electronic dynamics. Here, the relevant questions include: angle (polarization), frequency, and intensity dependent ionization rates; rates from molecular-orbital channels; and the downstream dynamics following ionization. There are numerous approaches to studying the ionization rates of multi-electron atoms and molecules. The simplest is perhaps the single active electron (SAE) approximation, which is mostly used in the context of the strong field approximation (SFA),[21] where the electron-electron interactions are neglected (replaced with a pseudopotential) and the time-dependent Schrödinger equation is solved for a single electron coupled to the driving field.[22,23] Another common approach is Keldysh-Feisal-Reiss (KFR)[24–26] and molecular-orbital Ammosov-Delone-Krainov (MO-ADK),[27,28] which are both extensions of Keldysh[24] theory and have been extensively applied to ionization rates.[21,29–32] MO-ADK has become the workhorse of ionization calculations including angle-dependent and molecular-orbital dependent rates. MO-ADK, however, may fail to predict accurate rates when ion-electron interactions and above threshold ionization (ATI) are required, although extensions have been developed for static ATI.[33] These models, nonetheless, use a SAE model that does not take many-electron effects into account.

On the other hand, various time-dependent electronic structure techniques have been applied to strong-field ionization, including time-dependent Hartree-Fock (TDHF),[34]

a)Electronic mail: klopata@lsu.edu

time-dependent density functional theory (TDDFT),[35–46] and time-dependent configuration interaction singles (TD-CIS).[47,48] These methods incorporate electron/electron interactions in an approximate way, but potentially suffer from breakdowns in the theory for strong-fields, basis set limitations, and increased simulation cost. TDDFT, in particular, offers a very promising trade-off between accuracy and favorable scaling with system size for strong-field ionization of molecules, and has been applied to systems ranging from small atoms like helium to large molecules like benzene.[38,42,43] Moreover, TDDFT has shown promise for excited state response properties such as double excitations[49] and excited state absorption,[50] although breakdown in the adiabatic (local-in-time) functional can be problematic.[51,52]

One critical drawback is that the accuracy of a TDDFT simulation hinges on the choice of DFT functional, which is, in general, not systematically improvable. Various studies have shown that one crucial ingredient for strong field ionization (SFI) is the correct long-range $1/r$ form of the potential, which can be accomplished by splicing corrections onto traditional DFT functionals, for example LB94 and CS00.[53,54] These correction approaches have been used for better description of the asymptotic behavior of the Coulomb potential, leading to improved ionization potentials and change transfer excitations.[53–56] A second important property is reduced self-interaction, where electrons spuriously self-repel themselves due to an imperfect DFT exchange-correlation functional. Self-interaction corrected (SIC) DFT in conjunction with asymptotic corrections has been successful in capturing strong-field ionization in molecules. In this work we will instead use tuned-range separated functionals designed for charge-transfer excitations, which require no *ad hoc* corrections or parametrization from experiment. This class of functionals has been used previously for SFI. Studies of D_2 Coulomb explosion,[57] for example, found that long-range corrected TDDFT[58] and TDHF gave similar results. This suggests that reduced self-interaction is likely more important than correlation for SFI, but the validity for larger molecules is less well-studied.

Another limitation of TDDFT involves the basis sets. Plane-waves or a grid representation are natural for strong-field ionization, but typically require pseudopotentials (frozen electrons) for the low lying molecular orbitals, which limits their utility for cases where core level orbitals contribute to the ionization. Moreover, evaluation of hybrid (Hartree-Fock admixture) DFT functionals is significantly more costly versus atom-centered basis sets, thus most plane-wave or grid approaches use some variants of local density (LDA) or generalized gradient (GGA) approximations.

In this paper, we present a new methodology using tuned range-separated real-time time-dependent density functional theory (RT-TDDFT) using atom-centered Gaussian-type orbitals (GTOs) and a spatial complex absorbing potential (CAP). The use of tuned range-separated functionals remedies many of the deficiencies of TDDFT and has the correct asymptotic form of the potential, reduced self-interaction errors, and improved ionization potentials, all without experimental parametrization. Moreover, these all-electron simulations make no assumptions about the molecular orbitals at play and are able to capture ionization from all MO channels. The remainder of the paper takes the following form: In Sec. II we detail the technical approach; in Sec. III we present validation against three well-studied systems: the hydrogen atom, molecular nitrogen (N_2), and iodoacetylene (HCCI); and we summarize in Sec. IV. All units used in this paper are in atomic units (a.u.), unless stated otherwise.

II. METHODS

In this section, we outline the approach to using Gaussian basis sets and tuned-range separated TDDFT for computing strong-field ionization in molecules. All methods were implemented in a development version of NWChem.[59] Broadly, this involves five steps:

1. Choice of an atom-centered basis suitable for ionization (Sec. II A).
2. Tuning a range-separated functional for the molecule of interest (Sec. II B).
3. Construction of a spatial complex absorbing potential which is projected onto the atom-centered basis (Sec. II C).
4. Real-time propagation using range-separated TDDFT (Sec. II D).
5. Extracting total and molecular orbital contributions to the ionization rates from the time-dependent density matrix (Sec. II E).

A. Basis sets

Atom-centered basis sets, also known as linear combination of atomic orbitals (LCAOs), offer many advantages for molecular calculations including efficient evaluation of the two electron integrals, a well developed library of basis sets, and ability to perform all-electron simulations (e.g., X-ray absorption studies). As a result, they are nearly ubiquitous in molecular quantum chemistry simulations. The LCAO approach, however, has severe problems for capturing ionization dynamics due to the limited spatial extent of the Gaussian basis functions far from the molecule and inability to describe the ionized wavepacket. Nevertheless, the efficiency of LCAOs for evaluating hybrid functionals makes this approach tempting for TDDFT ionization studies.

On the surface, a very large diffuse basis set might possibly suffice, but in practice simply extending an even-tempered basis requires a prohibitively large number of functions with a large number of linear dependencies, which negates the efficiency gains over alternates like plane-waves. This is a consequence of the fact that basis sets engineered for energy calculations (e.g., Pople[60] or correlation consistent Dunning-style basis sets[61]) converge very poorly for properties far from the nuclei. A promising alternative is to instead augment traditional basis sets with auxiliary diffuse functions designed explicitly to capture ionization. Schlegel and co-workers have recently developed this "absorbing basis set" approach to capture ionization rates in molecules using time-dependent configuration interaction singles (TD-CIS) with excellent agreement with experiment.[48,62] In this paper, we

use the "medium" absorbing basis and "large" absorbing basis from Ref. 48, which we denote with an "&" and "&&" suffix, respectively, in conjunction with Dunning-type correlation consistent basis sets, i.e., the correlation-consistent valence triple-zeta singly augmented basis with an auxiliary medium absorbing basis will be denoted "aug-cc-pVTZ&." For the case of H-atom calculations, for example, there are 68 diffuse basis functions in & and 176 in &&, for a total of 91 and 199 for "aug-cc-pVTZ&" and "aug-cc-pVTZ&&," respectively.

Additionally, an LCAO approach actually becomes increasingly suitable for capturing ionization dynamics as the external field strength increases, provided only local dynamical information is required, i.e., one is not interested in the propagation of the free electron wavepacket, but only in the dynamics near the molecule. In this case, the outgoing charge can be removed with a complex absorbing potential (CAP) positioned just outside the tunnel length. This is discussed in Sec. II C. Although projection of an LCAO basis onto a CAP can introduce spurious "auto-ionizing" due to overlap of the ground state with a spatial complex absorbing potential, in the weak-field case this leakage can be corrected for, and for strong fields this leakage rate is orders of magnitude slower than the physical rate. This issue is discussed in detail in Secs. II C and III A. Finally, applying a high intensity field to a system bends the Coulomb barrier (reduces the tunnel length) which reduces the volume of space around the molecule that needs to be spanned by the basis set. As a result, broadly speaking for a given basis set, basis set limitations should decrease with field strength. Basis set convergence tests bear this out. As will be shown in Sec. III C for field intensities relevant to high harmonic generation, this LCAO approach is adequate.

B. Tuned range-separated functionals

In TDDFT, the interacting N electron system is treated as N non-interacting systems, with an additional exchange-correlation potential V_{xc} containing all interactions lost by this approximation. The time dependent Kohn-Sham equation is given by

$$i\frac{\partial\psi_j(\boldsymbol{r},t)}{\partial t} = \Big[-\frac{1}{2}\nabla_j^2 + V_0(\boldsymbol{r},t) + V_{\mathrm{H}}[n](\boldsymbol{r},t) + V_{\mathrm{xc}}[n](\boldsymbol{r},t) - \boldsymbol{D}\cdot\boldsymbol{E}(t)\Big]\psi_j(\boldsymbol{r},t), \quad (1)$$

where $V_0(\boldsymbol{r},t)$ contains the electron-nuclear attraction, $V_{\mathrm{H}}[n](\boldsymbol{r},t)$ is the Hartree potential (mean-field electron-electron repulsion), and $\boldsymbol{D}\cdot\boldsymbol{E}(t)$ is the dipole electric field coupling, where we have assumed a spatially uniform field across the molecule. The exchange-correlation potential V_{xc} is typically some approximate functional of the density and/or the wavefunction. As will be shown in Sec. II, the choice of V_{xc} has a drastic effect on ionization rates, largely due to two types of errors present in most pure and hybrid DFT functionals: delocalization error, and an incorrect long-range asymptotic form of the ground state Coulomb potential.

Delocalization errors arise from spurious self-interaction of the electrons with themselves due to the approximate nature of the exchange-correlation functional.[63] In many cases self-interaction errors become more important for systems with fewer electrons, such as the extreme case of a self-repelling lone electron in a hydrogen atom. The opposite can also be true, such as delocalization errors leading to increasingly nonphysical polarization of conjugated molecules as the system size increases. In the context of strong-field ionization, the rates are delicately sensitive to the charge distributions and their response to the field. The results are thus expected to be susceptible to delocalization errors, even more so than bound → bound excited states calculations. As pure DFT functionals typically over-delocalize due to improper description of exchange, they are predicted to overestimate ionization rates. Hartree-Fock (HF), on the other hand, has exact exchange but no correlation, which tends to result in over-localization of the charge. HF is thus expected to underestimate strong-field ionization rates. Moreover, self-interaction errors will result in incorrect rates for intense fields, as during the course of a simulation fractions of an electron will be ionized each cycle of the laser. The time-dependent response will thus be artificially a function of the partial charge of the system, which manifests as incorrect ionization rates. This is related to the so-called "straight-line" behavior of the DFT functional, where a well-behaved functional should have a linear energy vs partial charge plot, with derivative discontinuities at integer numbers of electrons. This is explored further in Sec. III C.

The long-range asymptotic form of the potential is also expected to have an effect on DFT ionization rates. Pure DFT and global hybrid functionals have the incorrect long-range $1/r$ form of the potential between the parent ion and the ionized electron, which results in the well-known failure of most DFT functionals for describing charge transfer excitations.[64] There has been much success in this direction through spliced asymptotic corrections (e.g., LB94,[65] CS00[54]) which yields improved ionization rates. A more elegant solution is to use range-separated functionals, where the short-range interactions are treated using a DFT functional, the long-range interactions are treated with Hartree-Fock (which has the correct $1/r$ potential), and smoothly varied between[66]

$$\frac{1}{r_{12}} = \frac{\alpha+\beta\,\mathrm{erf}(\mu r_{12})}{r_{12}} + \frac{1-[\alpha+\beta\,\mathrm{erf}(\mu r_{12})]}{r_{12}}. \quad (2)$$

The choice of how quickly the potential switches from DFT to HF is essentially phenomenological, but can be chosen in an "*ab-initio*" way via self-consistent tuning of the function such that the ionization potential (IP) calculated via self-consistent field (ΔSCF) is the same as the Koopmans' IP (eigenvalue of the HOMO).[66] This requires minimizing the object function

$$J = |E(\Delta\mathrm{SCF}) - E(\mathrm{Koopmans})| \quad (3)$$

$$= |E_{\mathrm{cation}} - E_{\mathrm{neutral}} + \epsilon_{\mathrm{HOMO}}|\,. \quad (4)$$

In practice, this prescription typically results in ionization potentials for molecules within a few percent of experiment,[67–69] yields drastically improved charge-transfer excitation energies, remedies problems with TDDFT for large molecular systems,[70,71] and enables TDDFT to capture above ionization valence and above-edge X-ray spectra without input from experiment.[72] Moreover, as a consequence of this

tuning, these functionals generally have significantly improved straight-line behaviors, and can even be tuned to ensure this property is satisfied.[73] On the other hand, this tuning prescription is system (and potentially geometry) dependent and is thus not suitable for simulations incorporating nuclear dynamics. Moreover, since this tuning prescription depends entirely on ground state properties, the functional is universal across laser intensities.

In this paper, we use the tuned LC-PBE* functional, which consists of pure PBE in the short range and pure HF in the long range ($\alpha = 0$ in Eq. (2)). This requires a relatively simple 1D tuning by varying the range-separation parameter μ to minimize the object function in Eq. (4). An improvement would be to include a global hybrid contribution by varying both μ and α and perform a 2D tuning (see, e.g., Refs. 66, 68, 74, and 75). Application of tuned-range separated functionals to strong-field ionization dynamics is, at first glance, a natural extension of charge-transfer and above threshold ionization TDDFT, but hinges on an efficient and accurate atom-centered basis set approach for practical simulations of molecules.

C. Complex absorbing potential (CAP)

Due to finite simulation sizes, a complex absorbing potential (CAP) is used to emulate an infinite simulation box by removing outgoing charge following ionization. Here, a time-independent imaginary position-dependent potential is added to the perturbed Hamiltonian making its eigenvalues complex, which also makes the Hamiltonian non-Hermitian. In a real-space representation

$$H(\boldsymbol{r},t) = H_0(\boldsymbol{r},t) - i\Gamma(\boldsymbol{r}), \tag{5}$$

where $H_0(\boldsymbol{r},t)$ is the molecular Hamiltonian including the interaction with the field, and $i\Gamma(\boldsymbol{r})$ is an imaginary spatial potential, which is zero in the middle of the simulation and smoothly increases at the boundary such that the bound states are unaffected but charge far from the molecule is removed. An insufficiently strong CAP might not remove all charge causing artificial reflections from the simulation box, whereas conversely an overly sharp CAP might cause reflections from the potential itself. For this work the spatial CAP was chosen to be the sum of sigmoidal potentials centered on each atom in the molecule

$$\Gamma(\boldsymbol{r}) = \sum_{a=1}^{N_{\text{atoms}}} \Gamma_a(\boldsymbol{r}), \tag{6}$$

where

$$\Gamma_a(\boldsymbol{r}) = \begin{cases} 0, & R \le R_0, \\ \Gamma_0 \sin^2\left[\dfrac{\pi}{2W}(R - R_0)\right], & R_0 < R < R_0 + W, \\ \Gamma_0, & R \ge R_0 + W. \end{cases} \tag{7}$$

Here R is the distance from the atom, R_0 is the starting position of the CAP from the atom, W is the width of the CAP (before it reaches its maximum), and Γ_0 is the maximum value of the imaginary potential. In practice, the results are typically insensitive to W and Γ_0 but sensitive to the starting position of the CAP R_0. Ionization rates over a range of CAP starting distances are computed, and the value is chosen where the rates are invariant with respect to R_0. This optimal CAP geometry might be somewhat dependent on intensity, but we observed the results to be insensitive to intensity, thus we chose the CAP based on the middle of the intensity range of interest. At the resultant distances ($R_0 \sim 7$ Å), even though the CAP removes the electron density there is still a Coulomb interaction between the parent ion and the electron. To integrate this approach into an atom-centered basis set TDDFT approach, the CAP is first built on a spatial grid before being projected onto the atomic orbitals (AOs) to yield a potential which is added to the AO basis Fock matrix,

$$\begin{aligned} \Gamma_{\mu\nu} = \langle\mu|\Gamma(\boldsymbol{r})|\nu\rangle &= \int d\boldsymbol{r}\, \phi^*_\mu(\boldsymbol{r})\Gamma(\boldsymbol{r})\phi_\nu(\boldsymbol{r}), \\ \psi_a(\boldsymbol{r}) &= \sum_i C_{ai}\, \phi_i(\boldsymbol{r}). \end{aligned} \tag{8}$$

Here, $\Gamma(\boldsymbol{r})$ is constructed on a cubic Cartesian grid and $\phi_i(\boldsymbol{r})$ are the Gaussian-type orbitals. The CAP → basis set projection is done on a Cartesian grid, which in practice requires sufficient density to ensure a good projection. In order to check that this projection was successful, the diagonal matrix elements of the overlap were confirmed to be nearly unity

$$S_{\mu\mu} = \int d\boldsymbol{r}\phi^*_\mu(\boldsymbol{r})\phi_\mu(\boldsymbol{r}). \tag{9}$$

In practice the results were insensitive to the Cartesian grid parameters provided a sufficiently large box with a sufficient density of points was used.

Finally, as the CAP makes the Hamiltonian non-Hermitian, in principle the ground state wavefunction and resulting complex eigenvalues should be computed using a non-Hermitian self-consistent field (SCF) procedure before time propagation. This is cumbersome for an electronic structure code like NWChem, which is coded for Hermitian operators, so we instead computed the ground state using imaginary time propagation[76] starting from the CAP-free wavefunction. The occupied molecular orbital eigenvalues were observed to have a negligible imaginary part (infinite lifetime). Moreover, as the virtual orbitals do not contribute to the ground state energy in DFT, they were likewise not appreciably affected by the imaginary time energy minimization. We verified that the imaginary time converged and Hermitian SCF converged initial conditions gave essentially identical dynamics. Thus, for simplicity we used the Hermitian SCF ground state as the initial condition for time propagation.

D. Time propagation

For the purposes of ionization calculations, Eq. (1) is conveniently solved by integrating in time, i.e., "real-time" TDDFT,[77–79] although frequency-based complex scaling methods can alternatively be used to compute excited state lifetimes directly.[80,81] In a Gaussian basis this is typically done using the corresponding von Neumann equation of motion

$$i\frac{\partial \boldsymbol{P}'(t)}{\partial t} = [\boldsymbol{F}'(t), \boldsymbol{P}'(t)], \tag{10}$$

where $P'(t)$ and $F'(t)$ are the density and Fock matrices, respectively, in an appropriate orthogonal basis (e.g., using

canonical orthogonalization[82]). The corresponding quantities in the atomic orbital (AO) basis are denoted without a prime: $\boldsymbol{P}(t)$, $\boldsymbol{F}(t)$. Eq. (10) can then be integrated in time under the influence of an external field. Here we use an exponential-midpoint with self-consistent interpolation (i.e., a second order Magnus integration[83]) with $\Delta t = 0.2$ a.u. = 4.84 as. We use the real-time TDDFT implementation in a development version of NWChem.[59] For an overview of real-time TDDFT see the review by Isborn,[84] for algorithm and computational details of GTO real-time TDDFT, see Refs. 85–88 and for specific technical details of this implementation, see Refs. 72, 89, and 90.

The laser field can take any oscillating form, but we will typically take a quasi-monochromatic continuous-wave (CW) field of arbitrary linear polarization such that the field components in terms of polar (θ) and azimuthal angles (ϕ) with respect to a molecular axis are

$$E_x(t) = E_0\mathcal{E}(t)\sin(\theta)\cos(\phi)\sin(\omega_0 t), \tag{11a}$$

$$E_y(t) = E_0\mathcal{E}(t)\sin(\theta)\sin(\phi)\sin(\omega_0 t), \tag{11b}$$

$$E_z(t) = E_0\mathcal{E}(t)\cos(\theta)\sin(\omega_0 t), \tag{11c}$$

where ω_0 is the frequency of the field and E_0 is the amplitude of the laser. The pulse envelope $\mathcal{E}(t)$ was chosen to be a smoothly increasing shape to limit excitations caused by the pulse, as specified in the results.

E. Extraction of ionization rates

To extract the ionization rate, the expectation value of the total electronic charge $q(t)$ of the system is computed as a function of time

$$q(t) = \mathrm{Tr}\left\{\mathrm{Re}[\boldsymbol{P}(t)]\boldsymbol{S}\right\}, \tag{12}$$

where $\boldsymbol{S}$ and $\boldsymbol{P}(t)$ are the overlap matrix and time-dependent density matrix in the atomic orbital basis, respectively. This is akin to integrating the outgoing flux over all angles. Additionally, by assuming ionization only occurs along the axis of the light polarization, we can vary the polarization to determine the angle-dependent ionization rates. There is some flexibility in how ionization rates are defined, including slope of the charge curve or total charge lost divided by pulse time. For our purposes, however, the charge plots are exponential for strong fields so we instead computed the rates by fitting the number of electrons $n(t) = -q(t)$ to an exponential

$$n(t) = e^{-s(t-t_0)} + n_0 - 1, \tag{13}$$

where n_0 is the number of electrons before ionization, t_0 accounts for the time delay due to the envelope ramping up, and the exponential time constant s corresponds to the ionization rate. The form in Eq. (13) implicitly assumes single electron ionization as $t \to \infty$ and is thus only valid for partial electron ionization in multi-electron systems.

Finally, to compute the ionization rates from each molecular orbital channel, the time-dependent density matrix can be projected onto the ground state Fock matrix

$$n_k(t) = \left(\boldsymbol{C}'_k\right)^{\dagger}\boldsymbol{P}'(t)\boldsymbol{C}'_k, \tag{14}$$

where $n_k(t)$ are the MO occupations and $\boldsymbol{C}'_k$ is the matrix of eigenvectors of the ground state Fock matrix in the orthogonal basis. This projection is only valid for the field-free case as strong fields may induce instantaneous Stark shifts, thus the populations are only computed when the electric field crosses zero. Assuming the laser field causes no excitations to virtual orbitals, the rates of ionization from each MO can then be computed via the change in the population of the MO.

III. RESULTS

Initially we validated the approach against previously reported single electron simulations. As single electron systems have no electron/electron interactions, from a theory standpoint they can be treated exactly which allows us to verify the accuracy of this atom-centered basis set approach. In our framework, these simulations were performed using single electron time-dependent Hartree-Fock where the self-interaction exactly cancels, essentially yielding time-dependent Schrödinger equation results in a GTO basis. The idea behind these tests is twofold: (i) Confirm convergence with basis set, (ii) determine CAP position by ensuring ionization rate is insensitive to CAP placement.

A. Hydrogen atom quasi-static ionization

We first compute intensity-dependent static (DC) ionization of hydrogen, using the same basis set (aug-cc-pVTZ&, & = medium absorbing basis) and CAP starting position of $R_0 = 5.25$ Å as Ref. 48. The spatial CAP grid was $30 \times 30 \times 30$ Å^3 with $256 \times 256 \times 256$ grid points, the CAP potential max was $\Gamma_0 = 10$ hartree, and the width was $W = 10$ Å. For the laser, we used a quasi-static z-polarized electric field with an envelope function taken to be smoothly increasing to minimize excitations

$$\mathcal{E}(t) = \begin{cases} 0, & t < 0, \\ E_0(1 - (\frac{t}{t_c} - 1)^4), & t \le t_c, \\ E_0, & t > t_c, \end{cases} \tag{15}$$

such that the field reaches its maximum value E_0 at t_c, which was taken to be 558 a.u. (13.5 fs) for all simulations. For H-atom cases where the quasi-static field is applied, $E(t)$ does not have a $\sin(\omega_0 t)$ component to it. The time-dependent electric field and the resulting expectation value of the norm (number of electrons) are shown in Fig. 1. Once the electric field reaches its maximum, the norm decreases linearly due to charge being removed by the CAP. Additionally, at early times there is a small non-physical charge leakage due to finite overlap of the CAP with the ground state, which is an artifact of the atom-centered basis sets. This spurious "auto-ionizing" was found to be insignificant compared to the physical ionization at moderate to high field intensities, but resulted in significantly overestimated rates at low intensities. To compensate for this, the leakage rate was determined via a linear fit of the time-dependent norm computed without a laser field, which was then subtracted from $n(t)$ for the ionization

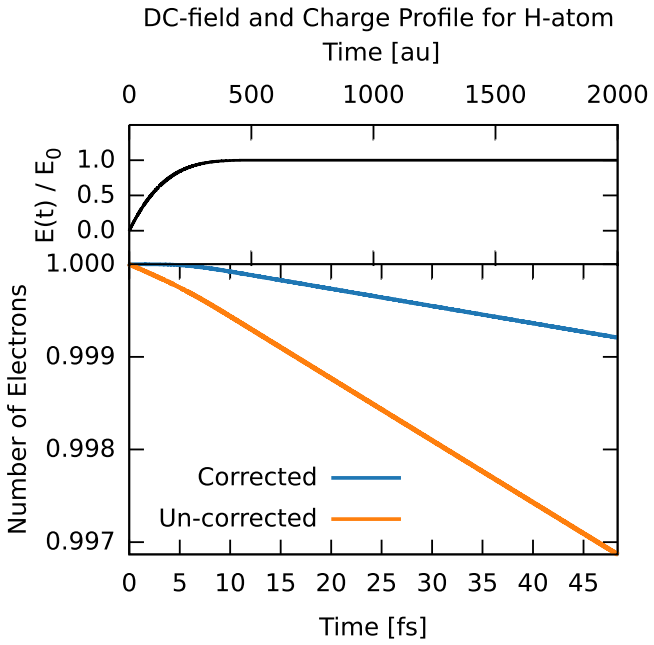

FIG. 1. Quasi-static (DC) ionization of a hydrogen atom with field amplitude $E_0 = 0.03$ a.u. For this relatively low intensity laser field (top), the spurious auto-ionizing due to overlap of the ground state with the CAP results in an artificially fast ionization rate (bottom, orange). Correcting for this (bottom, blue) yields the physical ionization rate, which is in agreement with time-dependent Schrödinger equation simulation results (see Fig. 2).

simulations. This approach was applied to all simulations in this paper.

The intensity-dependent ionization rates were then computed from an exponential fit of the expectation value of the charge via Eq. (13) for various values of E_0, as shown in Fig. 2. The result agrees well with TDSE results over a range of amplitudes spanning 0.03 a.u.–0.1 a.u., demonstrating the validity of the basis set and CAP. Note that the lower intensity ionization rates ($E_0 \leq 0.05$ a.u.) required the leakage correction outlined above, as the leakage rates were on the same order as the physical ionization rates (see Fig. 1), whereas for higher intensities the correction was not necessary. Finally, to check basis set convergence, the above prescription was repeated for a range of basis sets including single to quadruple zeta and single to quadruple augmented Dunning-type basis sets with auxiliary medium (&) or large (&&) Schlegel absorbing basis functions. These tests demonstrated that aug-cc-PVTZ& basis yields effectively converged results. For comparison, the intensity dependent DC rates for the smallest and largest basis are shown on Fig. 2.

B. Hydrogen atom AC ionization

Next, the ionization rate of a hydrogen atom subjected to an oscillating (AC) field was calculated, which is a further test of the basis sets and CAP, as this is in principle an exact simulation. To compare with time-dependent Schrödinger equation (TDSE) results,[92] 40 cycles of 1064 nm light ($\omega_0 = 0.043$ a.u.) was applied for a range of field intensities, with the rates computed via exponential fit of the norm, as in the static (DC) case. To be consistent with Ref. 93 the following ramped envelope was used:

$$\mathcal{E}(t) = \begin{cases} 0, & t < 0, \\ \sin^2(\pi t/2\tau), & 0 \leq t \leq \tau, \\ 1, & t > \tau, \end{cases} \tag{16}$$

where $\tau = 10\pi/\omega_0$. Two basis sets were used, a modest set (aug-cc-pVTZ&) and a large set (q-aug-cc-pv5Z&&) and the CAP starting position was chosen by determining a region where the rate is insensitive to R_0. The spatial CAP grid parameters were the same as for the DC case, except for the R_0 value which we picked to be 7.125 Å. For the smaller basis set, for example, the ionization rate is insensitive over a range of CAP starting positions from 4-9 Å, as shown in Fig. 3. Note that the rates in the plot are in a logarithmic scale to better emphasize the range of rates and for better visualization of the insensitive region. This was computed using the $I = 10^{14}$ W/cm^2, but the optimal R_0 was found

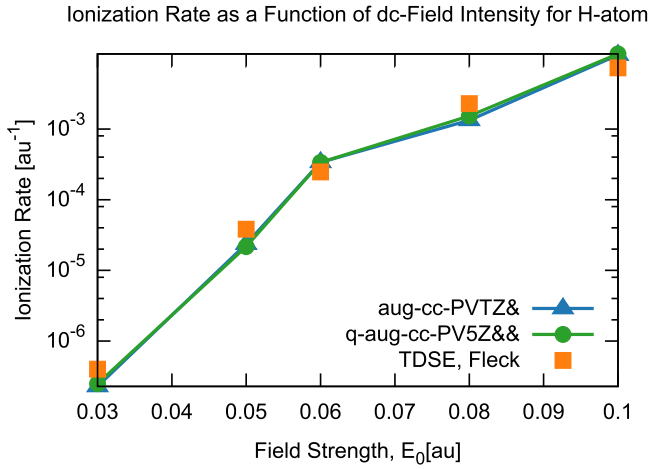

FIG. 2. Intensity dependent ionization rates for a hydrogen atom under a quasi-static electric field. This Gaussian-type orbital (GTO) basis set approach quantitatively agrees with the time-dependent Schrödinger equation (TDSE) by Fleck.[91]

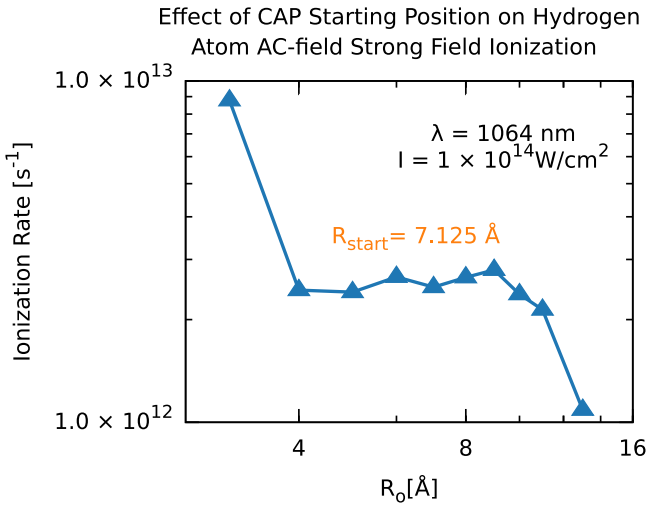

FIG. 3. Ionization rates as a function of CAP starting distance R_0 for a hydrogen atom under 1064 nm light with intensity 1×10^{14} W/cm^2. The rates are insensitive from $R_0 = 4$ to 9 Å, with an optimal R_0 chosen to be around mid-point in this region, which is ~7 Å.

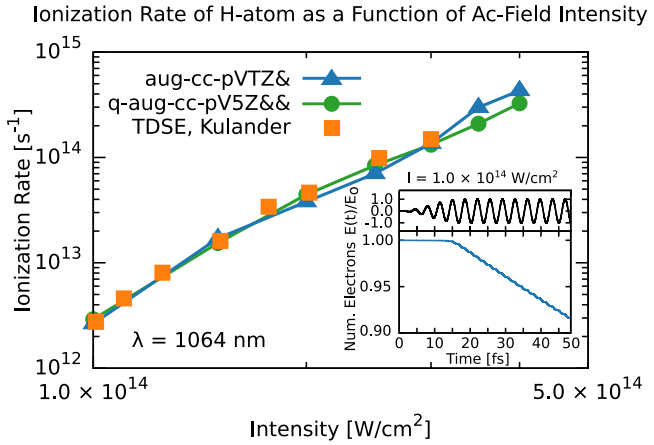

FIG. 4. Intensity-dependent ionization rates for a hydrogen atom under quasi-continuous wave 1064 nm light for a small basis set (aug-cc-pVTZ&) and a large basis set (q-aug-cc-pV5Z&&). The single electron atom-centered basis set results agree well with TDSE results,[92] with slight deviations due to basis set limitations. Inset: Time-dependent charge for aug-cc-pVTZ& basis and $I = 1\times10^{14}$ W/cm^2.

to be insensitive to intensity. Moreover, similar results were obtained for the larger basis set, thus we calculated the intensity dependence using the small basis. As before, spurious leakage was compensated for by subtracting the field-free ionization. An example corrected time-dependent norm is shown in the inset in Fig. 4.

The resulting rates (main plot in Fig. 4) are in good agreement with TDSE rates both for weak and strong field cases. For the weakest intensity (1×10^{14} W/cm^2) the norm drops linearly and approximately 0.1 electrons are removed after the full simulation, whereas for the highest intensity (2.5×10^{14} W/cm^2) essentially one full electron is completely ionized.

C. Molecular nitrogen

Next we discuss strong-field ionization in N_2, which is one of the most well-studied systems in strong-field physics, both experimentally and theoretically, and offers a good test case for the accuracy of tuned range-separated TDDFT for ionization rates. The geometry was determined by optimizing with aug-cc-pVTZ/PBE0 with the molecular axis along the z-direction, yielding a bond length of 1.089 Å. The tuned LC-PBE* functional varies smoothly from PBE at the short-range to HF at the long range, with the parameter μ (the attenuation parameter in Eq. (2)) determined by minimizing the deviation between the SCF and Koopmans first ionization energy. To avoid convergence issues with large basis sets, we used aug-cc-pVTZ without the auxiliary absorbing basis functions for the tuning. The optimal range-separation parameter was found to be $\mu = 0.5775$ a.u.$^{-1}$ and the resulting ionization potential was 16.5 eV (experimental value 15.6 eV) as shown in Fig. 5 (Top).

Next, we explored the straight-line behavior of this functional, which is a measure of the delocalization error. Fig. 5(b) shows the resulting change in energy of N_2 as a function of partial electronic charge for Hartree-Fock, PBE, and LC-PBE*. The Hartree-Fock curve has a slightly convex

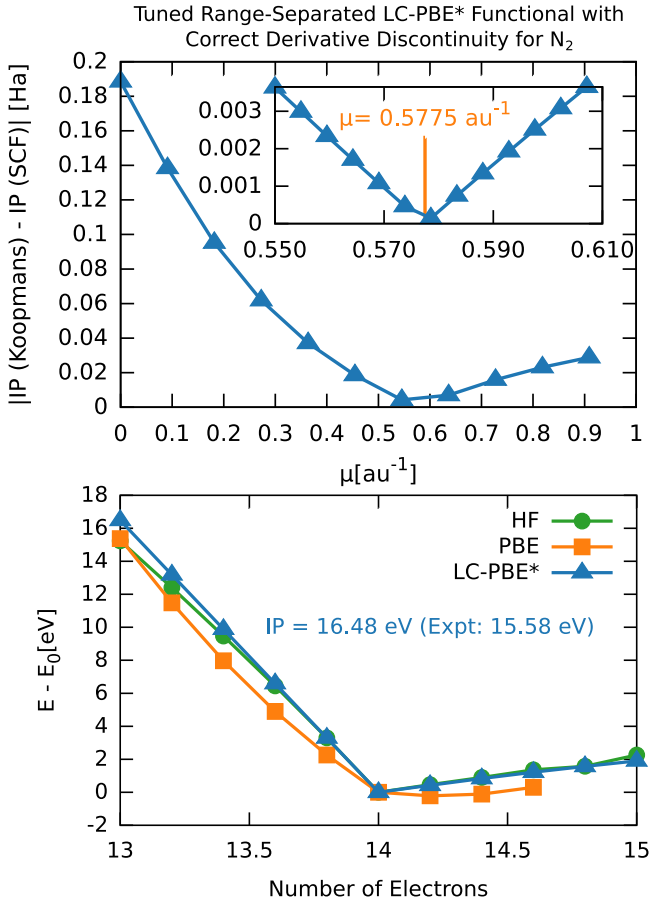

FIG. 5. (Top) Optimal tuning of the LC-PBE* for N_2. (Bottom) Straight line behavior for a range of functionals. The GGA functional PBE exhibits a concave shape due to over-localization, whereas the tuned LC-PBE* functional has the correct derivative discontinuity.

shape due to over-localization, the PBE curve is noticeably concave due to over-delocalization, and the LC-PBE* curve is essentially linear with a derivative discontinuity at $N = 14$. This straight-line behavior is indicative of a functional with reduced self-interaction errors. In the context of strong field ionization, a partially ionized molecule during a TDDFT simulation should have a response that is insensitive to the fractional electron number, at least until a full electron is ionized. Self-interaction errors, corresponding to a non-linear $E(n)$ curve, thus result in a non-physical fractional charge-dependent response, which manifests as erroneous ionization rates. Thus, from the straight-line plot in Fig. 5(b), LC-PBE* is expected to yield an improved response, whereas self-interaction errors due to partial electron numbers in PBE will lead to overly large ionization rates, as the partial electrons overly repel themselves. Conversely, due to lack of correlation HF will tend to underestimate the rates. These effects are in addition the incorrect asymptotic form of the potential in the PBE functional, and such self-interaction errors would likely remain an issue in alternate approaches such as asymptotically corrected local DFT approaches like LB94.[65]

In practice, the relative importance of self-interaction versus correlation effects depends on the system, as well as the laser frequency and intensity. To explore this we computed the z-polarized (on-axis) ionization rates of N_2

using the aug-cc-pVTZ& basis set and Hartree-Fock, PBE, and LC-PBE*. The spatial CAP was $25 \times 25 \times 25$ Å^3 with $200 \times 200 \times 200$ grid points. Γ_0 and W were picked to be 10 Ha and 10 Å, respectively. Here the laser frequency ω_0 was taken to be 0.057 a.u. (λ = 800 nm) and the field has an envelope function given in (Eq. (16)). The simulations were run for six optical cycles (650 a.u. total simulation time) to get a quasi-continuous wave response and the resulting ionization rates were computed from fitting an exponential to the decaying time-dependent system charge as outlined in Sec. II E. The leakage due to ground state overlap with the CAP was corrected by subtracting a linear fit to the time-dependent field-free norm, as with the hydrogen atom. The CAP geometry was optimized in the manner described for the hydrogen atom. Fig. 6 shows the dependence of the LC-PBE* ionization rate on CAP start R_0 for z-polarized (on-axis) $I = 2 \times 10^{14}$ W/cm^2 light, which yielded an optimal $R_{\text{start}} = 6.5$ Å. Similar optimal CAP positions were observed for HF, PBE, LC-PBE*, for all intensities considered, thus for consistency we used the same R_0 value for all calculations. Unlike in the hydrogen atom case, however, the rate is relatively insensitive to R_0 as the physical ionization rate is much greater than the non-physical leakage due to excessive overlap of the CAP with the ground state. Additionally, basis set convergence was checked for intensity $I = 2 \times 10^{14}$ W/cm^2 as per the DC hydrogen case, which confirmed the validity of the basis.

First, the effect of DFT functional on the ionization rates was explored within the PBE family of exchange-correlation functionals. Fig. 7 shows the resulting time-dependent norm for $I = 2 \times 10^{14}$ W/cm^2. The ionization-rate varies by a factor of ~20, which demonstrates the extreme sensitivity of strong-field ionization to the choice of functional. Pure Hartree-Fock, which has the correct ground state long-range Coulomb potential but lacks electronic correlation, exhibits the lowest rate due to over-localization of the electrons due to the lack of correlation. The pure DFT functional PBE, on the other hand, shows a 20× faster rate than HF due to over-delocalization. The PBE0 functional which contains a global admixture of HF has a rate between the pure DFT and HF limits. However,

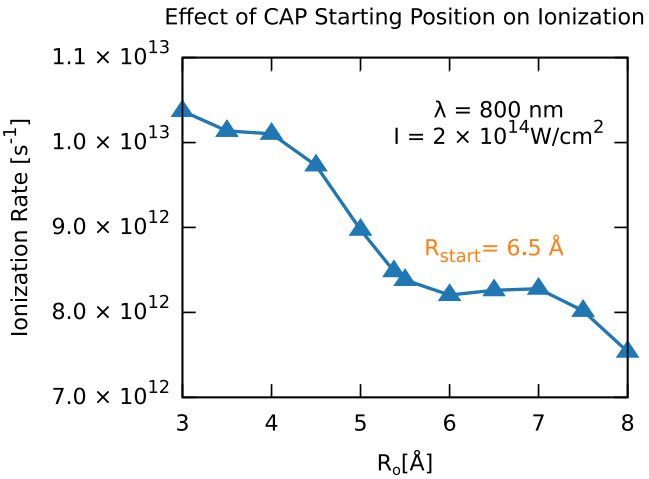

FIG. 6. Determination of the optimal CAP start distance for N_2 under $\lambda = 800$ nm $I = 2 \times 10^{14}$ W/cm^2 light and the LC-PBE* functional.

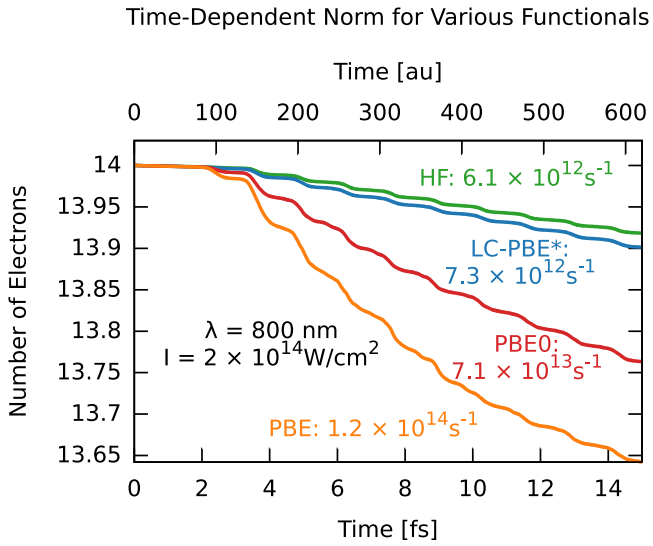

FIG. 7. Time-dependent norm for N_2 irradiated with $\lambda = 800$ nm, on-axis polarized, $I = 2 \times 10^{14}$ W/cm^2 light. The pure DFT functional (PBE) over-delocalizes the charge density, which overestimates ionization rates. Hartree-Fock over-localizes the density, which underestimates the rate. The range-separated LC-PBE* functional has reduced self-interaction errors as well as the exact long-range Coulomb potential, which yields a more accurate ionization rate.

neither the PBE nor PBE0 functionals properly describe long range (electron/ion) interactions, which is related to the well-known failure of TDDFT for charge transfer excitations. The tuned range-separated functional LC-PBE*, in contrast, which captures the electron correlation within the molecule, has reduced self-interaction error, and has the correct Coulomb interaction long-range, yielding a rate between HF and PBE0.

To assess the accuracy of this approach, intensity-dependent on-axis (z-polarized) ionization rates were computed and compared to molecular orbital strong-field approximation (MO-SFA) results that have been validated against experiment.[94] Below we show that for intensities spanning $1\text{–}4 \times 10^{14}$ W/cm^2 the LC-PBE* results are in excellent agreement with MO-SFA. This region roughly corresponds to the intensities in high harmonic generation experiments. Table I shows the resulting rates, along with MO-SFA (length gauge) and MO-ADK HF results. For these intensities the HF and LC-PBE* results have the overall best agreement with the MO-SFA results, whereas the PBE are significantly higher. This is likely a reflection of the self-interaction errors in the PBE functional. LC-PBE* has slightly better agreement than HF, which tends to slightly underestimate the rate, consistent with the lack of correlation, although this effect is less important than self-interaction errors.

Furthermore, we directly compare these results to experiments on unaligned N_2 samples. As this involves angle-averaged rates, thus we first compute the angle-dependent ionization. Fig. 8 shows the HF and LC-PBE* angle-dependent rates for $I = 1.5 \times 10^{14}$ W/cm^2, where the laser polarization was in the xz-plane ($\phi = 0$) with angle θ such that $\theta = 0$ corresponds to parallel (z-oriented) light and $\theta = 90°$ is perpendicular (x-oriented). For LC-PBE*, the qualitative shape is similar to previous studies[21,47,95,96]

TABLE I. Intensity-dependent ionization rates for N_2 with on-axis polarized light. The length gauge MO-SFA and the MO-ADK HF results are taken from Madsen and Kjeldsen.[94] Intensities in W/cm^2 and rates are in s^{-1}.

Intensity	TD-HF	TD-PBE	TD-LC-PBE*	MO-SFA LG	MO-ADK HF
1.00×10^{14}	2.69×10^{11}	6.19×10^{12}	4.10×10^{11}	1.50×10^{11}	2.80×10^{12}
2.00×10^{14}	6.08×10^{12}	1.19×10^{14}	7.31×10^{12}	7.00×10^{12}	2.20×10^{14}
3.00×10^{14}	2.24×10^{13}	1.47×10^{14}	3.23×10^{13}	4.40×10^{13}	1.40×10^{15}
4.00×10^{14}	8.15×10^{13}	1.57×10^{14}	1.46×10^{14}	1.30×10^{14}	4.30×10^{15}

with fastest ionization occurring for on-axis polarized light. Looking at the normalized angle-dependent rates (right plot), both LC-PBE* and HF agree quite well with the normalized experimental rates[97] (black curve), up to $\theta > 45°$ after which the HF rate becomes essential insensitive to light polarization. This is a consequence of the incorrect molecular orbitals in HF. The orbitals are ordered incorrectly with the two π^u orbitals being the highest occupied MO, and σ_z^g lower in energy. As a result, the contribution due to the σ_z^g orbital is significantly underestimated for off-axis polarized light. Moreover, ionizing from this MO is quite insensitive to θ due to the cylindrical shape of this orbital. In a way, the angular dependence of the ionization rate maps the MOs of N_2, where HF is qualitatively incorrect. LC-PBE*, on the other hand, has the correct ordering of the MOs in the ground state and thus gives a more reasonable picture of the angle-dependent ionization.

It is also interesting to note that the normalized LC-PBE* curve agrees quite well with the experimental curve and predicts the shape and ratio of parallel to perpendicular rates much better than either MO-SFA or MO-ADK.[98] Corkum and co-workers[97] measured the ratio of these rates at 1.5×10^{14} W/cm^2 and determined the ratio to be 2.3 ± 0.3 assuming the ionizing laser partially aligns the sample and 3.3 ± 0.4 without any realignment. LC-PBE* calculated ratio is in good agreement with experiment by giving 2.38, while HF gives 1.42. In comparison, MO-ADK[97] and MO-SFA[94] give 10 and 8, respectively. Similar agreement was found compared to TD-CIS[47] at 2×10^{14} W/cm^2 where the LC-PBE* ratio was observed to be 1.90 which is in close agreement. The experimental ratio at this intensity was shown to be about four.[96] These results demonstrate that LC-PBE* not only predicts the rates but also the angle dependence, whereas HF yields reasonable rates but incorrect angle dependence.

Next, the angle averaged rates were computed to facilitate comparison with experiment. Here we assumed a $\cos^2\theta$ distribution, thus the angle averaged rate is approximately the average of the parallel and perpendicular rates. To compare to experiment, which is typically reported in ion counts, in principle one must account for all various experimental parameters such as laser pulse shape, variation of intensity across the beam cross-section, and gas density. As is often done,[94] we simply normalize the angle-averaged result for each functional to match the experiment at the saturation intensity of 3×10^{14} W/cm^2. The resulting normalized curves are shown in Fig. 9. PBE drastically overestimates the rates due to over-delocalization of the charge density. HF and LC-PBE* appear to give similar total rates, consistent with previous studies on D_2.[57] They also agree well with experiment between 1–4 $\times$ 10^{14}, with HF slightly overestimating the rates. This is a result of the underestimated on-axis HF rates (see Table I) being corrected for by the drastic overestimation of the perpendicular rate due to the incorrect MO ordering. For weaker fields, however, the rates incorrectly level off due

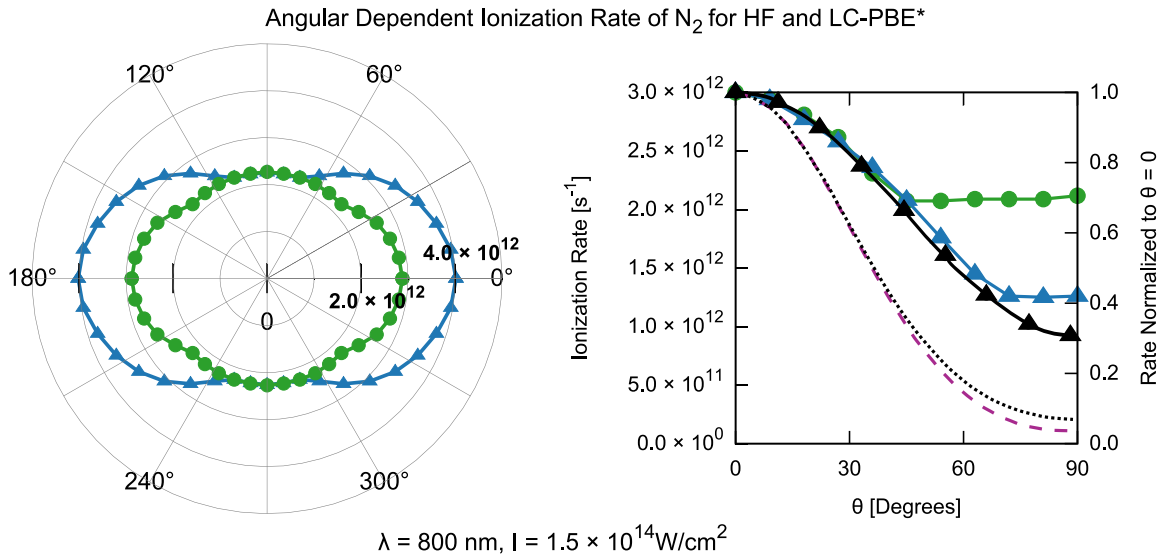

FIG. 8. Ionization rates of N_2 computed using HF (green circles) and LC-PBE* (blue triangles) as a function of light polarization angle (left). The corresponding linear plot (right) shows the angle-dependent rates normalized to the parallel ($\theta = 0$) rate for HF (green circles), LC-PBE*(blue triangles), experiment (black triangles), MO-SFA (dashed line), MO-ADK (dotted line). HF and LC-PBE* match the experiment well for small angles, but for $\theta > 45°$, HF unphysically becomes insensitive to angle due to the incorrect molecular orbital ordering.

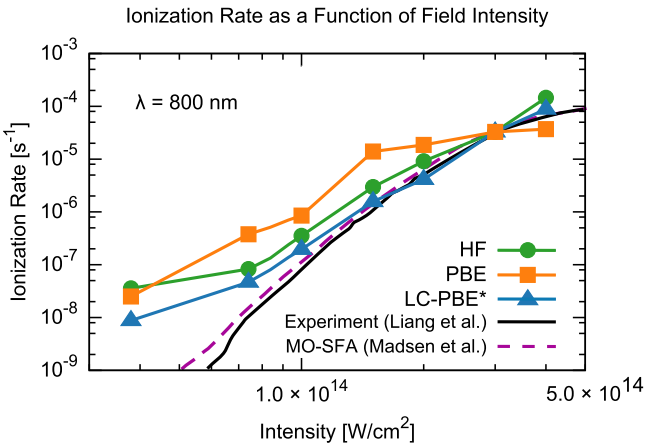

FIG. 9. N_2 angle averaged ionization rates as a function of field intensity computed using HF (green circles), PBE (orange squares), and LC-PBE* (blue triangles) normalized independently to experimental rate of 3×10^{14} W/cm^2. Experimental (black solid) curve digitized from Liang and co-workers[99] and MO-SFA LG (purple dashed) from Madsen and Kjeldsen.[94]

to basis set limitations and non-physical leakage that is not completely corrected for. For higher intensities, the rates start to saturate around 3×10^{14} W/cm^2, as evidenced by a change in the slope of the curve. This is also observed in experiment[99] and MO-SFA calculations.[94] At these extreme intensities the definition of a rate becomes ambiguous, as essentially one full electron is ionized per cycle. Given the consistency between HF and LC-PBE* at these high intensities, self-interaction issues do not appear to be important.

To further analyze the ionization rates, we separately computed ionization rates from each molecular orbital channel for intensity $I = 2 \times 10^{14}$ W/cm^2 and $\theta = 0$ and 90°. Fig. 10 shows the time-dependent population of the occupied orbitals, computed via projection onto the ground state at the times when the laser field is zero (see Eq. (14)). The projections are done in this way in order to ensure the orbitals are not Stark-shifted during the time the field is being applied, as Eq. (14) assumes non-shifted molecular orbitals. The norm decreases slightly even without an applied field due to non-zero overlap of the CAP with the occupied molecular orbitals. This physical ionization from each MO can be corrected for by adding back this non-physical leakage from each orbital as a post-processing step. These time-dependent plots have been corrected for the spurious auto-ionization by subtracting the linear fit of the field-free populations of each molecular orbital separately. This accounts for differing leakage rates from each MO. This analysis shows that for the case of on-axis light polarization ($\theta = 0$) the HOMO ($3\sigma_z^g$) is the highest contributor to the field, which is consistent with the z-oriented shape of this molecular orbital. The second highest contribution is from the $2\sigma_z^u$ (HOMO-3) which is likewise a z-oriented orbital. Next, the two $1\pi^u$ orbitals (roughly made of p_x and p_y orbitals) have the same rate since they are degenerate and perpendicular to the field. For the same field intensity but aligned perpendicular to the molecule ($\theta = 90°$, x-polarized), the HOMO ($3\sigma_z^g$) is still the dominant MO channel, but now the second highest contribution comes from the $1\pi_x^u$ orbital, which is parallel to the light polarization. Ionization from other MOs is negligible. These results are qualitatively consistent with previous TDDFT simulations.[100,101]

D. Iodoacetylene

Next we use the same approach to compute the molecular-orbital dependent strong-field ionization rates from iodoacetylene (HCCI), which was recently experimentally and computationally demonstrated to exhibit ionization triggered charge migration that could be observed with time-resolved high harmonic generation.[18] HCCI is a simple candidate molecule for charge migration studies due to its linear shape (experimental orientation or alignment), relatively high ionization potential (9.71 eV), and asymmetric charge density. Ionization from multiple MO channels results in a non-stationary electron state, and knowledge of these rates and their phases is crucial to reconstructing the attosecond dynamics on the resulting cationic molecule following ionization. To further validate our approach against the work done by Kraus and co-workers,[18] we compute the MO ionization rates of HCCI under $I = 1 \times 10^{14}$ W/cm^2 light of wavelengths (λ = 800 nm and

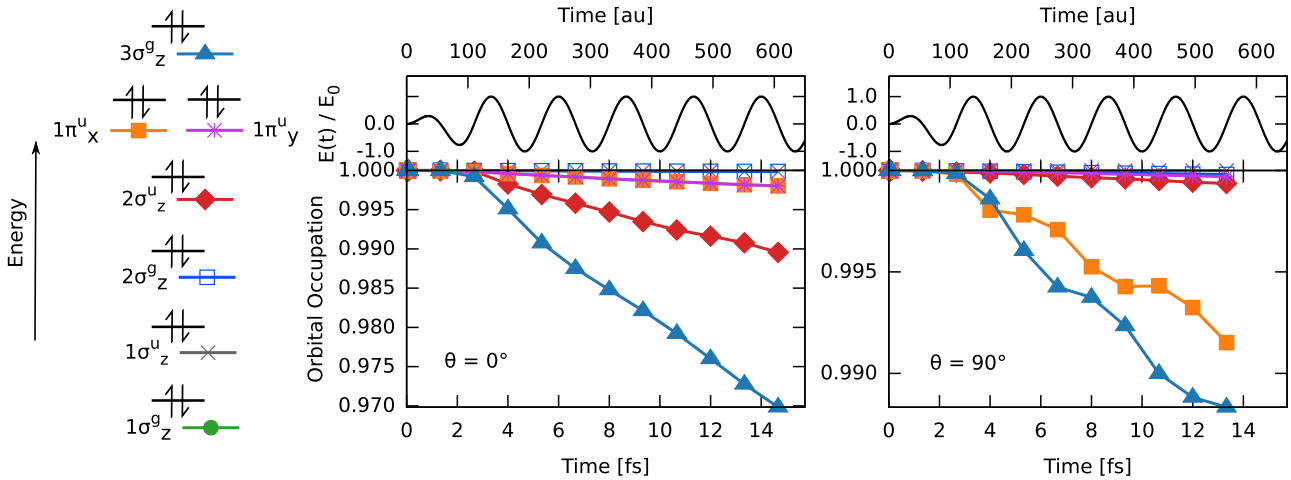

FIG. 10. Time-dependent molecular orbital occupations for z-aligned N_2 under $I = 2\times10^{14}$ W/cm^2 for z-polarized ($\theta = 0$, middle) and x-polarized ($\theta = 90°$, right) light. The molecular orbital diagram for the occupied levels of N_2 is shown on the left. In both polarization cases the HOMO ($3\sigma_z^g$) channel dominates with a significant contribution due to the $2\sigma_z^u$ and $1\pi_x^u$ for 0 and 90° alignments, respectively.

1300 nm) polarized perpendicular to the molecular axis. Here, 800 nm and 1300 nm light was chosen to match experimental parameters.[18] The HCCI geometry was optimized using the aug-cc-pVTZ basis on carbon and hydrogen, and the Stuttgart ECP28MDF-AVTZ[102] (28 electron pseudopotential) on iodine and the PBE0 functional, yielding bond lengths of R_{CH} = 1.064 Å, R_{CC} = 1.201 Å, and R_{CI} = 1.983 Å, with the molecular axis chosen to be along the z-direction. The LC-PBE* functional was then tuned in the same way as the N_2 molecule, resulting in an optimal range-separation parameter of $\gamma = 0.3663$ a.u.$^{-1}$, with a corresponding vertical ionization potential of 10.1 eV (experimental value[103] 9.71 eV).

For the ionization calculations, the CAP maximum was $\Gamma_0 = 10$ Ha, the width $W = 10$ Å, the spatial potential was $30 \times 30 \times 30$ Å^3 with $256 \times 256 \times 256$ grid points, and the CAP starting position was chosen to be $R_0 = 6.0$ Å as the rates were observed to be insensitive for CAP starting distances between 5 and 6.5 Å. The laser parameters were chosen to be the same as the N_2 case above: 10^{14} W/cm^2 ramped (Eq. (16)) continuous wave field applied for six optical cycles. As before, the molecular orbital populations were determined via projection on the ground state (Eq. (14)) when the laser field was zero, and corrected for spurious leakage by subtracting a linear fit to the field-free time-dependent populations. For projection purposes, in order to ensure the ground state molecular π orbitals were purely x and y aligned (rather than at an arbitrary angle), the system was converged in the presence of a weak static electric field created using two point charges +1 a.u. and −1 a.u. located at −100 Å and 100 Å in the y-direction. The energy was then minimized again without the charges, yielding purely x and y-oriented degenerate π orbitals.

First, the ionization anisotropy (ratio of the parallel to perpendicular rates) of HCCI was computed from the time-dependent norms. For both wavelengths the perpendicular ionization was faster than parallel (on-axis), with anisotropies of 0.9 and 0.8 for 800 nm and 1300 nm, respectively. The faster ionization with perpendicular light is a consequence of the molecular orbital shapes, where the four highest occupied orbitals are all xy-oriented, in contrast to N_2 where the highest rate of ionization occurs when the molecule is oriented in the same direction as the light polarization due to the orientation of the HOMO. Next we computed the channel-dependent rates. Fig. 11 shows the resulting time-dependent molecular orbital populations for $\theta = 90°$ (x-polarized, perpendicular to molecular axis) 800 nm and 1300 nm light. In both cases, the ionization is dominated by the π_x^g (HOMO) channel with some contribution due to the π_x^u (HOMO-2) channel. This is consistent with previously reported rates.[18] These results show that our approach based on tuned range-separated functionals can be extended to systems of interest for studying attosecond dynamics.

IV. CONCLUSIONS

In conclusion, we have developed an atom-centered Gaussian-type orbital (GTO) real-time TDDFT approach to strong-field ionization in molecules based on tuned range-separated hybrid (RSH) functionals for the correct long-range asymptotic Coulomb potential and reduced self-interaction errors, and a spatial complex absorbing potential (CAP) projected onto the GTO basis to emulate the continuum. The approach successfully captures the intensity and light polarization dependent ionization in the hydrogen atom, the nitrogen molecule, and iodoacetylene. More iodoacetylene work is underway to study the total ionization rates and the subsequent HHG process.

From a basis point of view, these modest-sized quantum chemistry GTO basis sets augmented with auxiliary diffuse functions[62] yield quantitative agreement with time-dependent Schrödinger equation results for DC and AC field ionization of hydrogen over a range of laser intensities. GTOs require complex absorbing potentials that start near the molecule, however, and are therefore unable to capture the ionized electronic wavepacket, for example. GTO basis sets enable efficient evaluation of hybrid DFT functionals (specifically range-separated hybrids), scale favorably to large molecules,[104] and can be applied to post Hartree-Fock

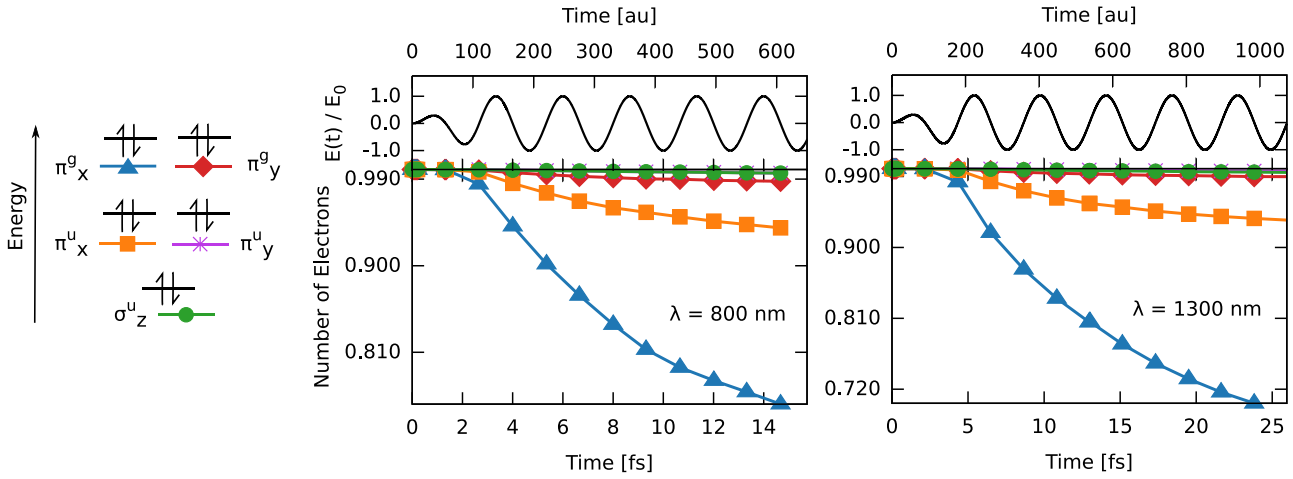

FIG. 11. Time-dependent molecular orbital populations of HCCI under $I = 1 \times 10^{14}$ W/cm^2 light polarized along the x-direction (perpendicular to the molecular axis) computed using LC-PBE*. The diagram for the five highest energy occupied molecular orbitals is shown on the left. For both 800 nm and 1300 nm, the ionization is dominated from the HOMO (π_x^g) and HOMO-2 (π_x^u).

wavefunction methods such as configuration interaction, active-space methods, and coupled cluster. On the other hand, GTOs suffer from basis set convergence issues and exhibit spurious "autoionization" due to overlap of atom-centered basis functions with the spatial CAP, which is especially prominent at lower intensities. Weak field rates can, however, be computed by correcting for this leakage rate.

In the context of strong-field ionization, tuned range-separated functionals have two distinct advantages over traditional DFT: correct $1/r$ asymptotic Coulomb form and improved straight line behavior. The asymptotic potential form is essential for long-range correction cation/ionized electron interactions, and local density (LDA) or generalized gradient (GGA) TDDFT with asymptotic correction terms such as LB94 and CS00 have been shown to give accurate ionization rates in atoms and diatomic molecules. Tuned RSH functionals offer a slightly more elegant solution as they are derived from well-defined energy functionals rather than *ad hoc* correction terms.

Tuned RSHs also remedy another limitation of traditional functionals, namely self-interaction error and spurious dependence of the molecular properties on partial electron number n. Subtle self-interaction errors manifest as drastic errors in strong-field ionization rates, especially for strong fields where large fractions of an electron are removed in a simulation. Thus, a function with the correct derivative discontinuity at integer n values, and a linear dependence of energy between, offers one of the best candidates for TDDFT rates over a wide range of laser intensities. The observed quantitative intensity dependent rates for N_2 support this interpretation. One possible future refinement to this approach is to tune the RSH using multiple ionization potentials, instead of just the first IP, which may increase the accuracy of the MO channel rates, and might increase accuracy under an extremely intense field, and even enable simulations where multiple electrons are ionized. It is interesting to note that IP is not a complete predictor of rate, e.g., for N_2, both HF and PBE have a smaller IP than LC-PBE*, but they yield slower and faster rates, respectively. TDDFT rates instead depend on many factors such as self-interaction, correlation errors, and the form of the long-range Coulomb potential, which differ from functional to functional.

Hartree-Fock, which also has the correct long-range asymptote and does not suffer from self-interaction, appears to give physically reasonable ionization rates, especially for the case where electron correlation is likely to be less important, such as high intensities. The HF angle-dependence in N_2, however, was found to qualitatively fail due to incorrect molecular orbital ordering, thus care should be taken when applying HF to molecular systems. Tuned LC-PBE*, in contrast, reproduced the experimental rates and angle-dependence.

Finally, it is important to also note that these are still ground state DFT functionals and using RSHs for strong-field simulations might still stress the adiabatic (local-in-time) approximation of the functional, especially for the high intensity cases, where the time-dependent density matrix differs significantly from the ground state. Adiabatic TDDFT for continuous resonant excitation or vertical excitation induced charge transfer, for example, is known to qualitatively fail due to inconsistent errors between the ground and excited states.[51,105] Here, however, the situation is different as the laser field does not induce appreciable virtual state populations, but instead essentially removes charge from occupied orbitals only. The errors in the functional for neutral vs partially ionized are likely to be less drastic than the excited state case.

ACKNOWLEDGMENTS

This work was supported by U.S. Department of Energy, Office of Science, Office of Basic Energy Sciences, under Award No. DE-SC0012462. Portions of this research were conducted with high performance computational resources provided by Louisiana State University (http://www.hpc.lsu.edu). Discussions with Erwin Poliakoff are gratefully acknowledged.

[1]F. Krausz and M. Ivanov, Rev. Mod. Phys. **81**, 163 (2009).
[2]E. Goulielmakis, Z.-H. Loh, A. Wirth, R. Santra, N. Rohringer, V. S. Yakovlev, S. Zherebtsov, T. Pfeifer, A. M. Azzeer, M. F. Kling, S. R. Leone, and F. Krausz, Nature **466**, 739 (2010).
[3]A. Wirth, M. T. Hassan, I. Grguras, J. Gagnon, A. Moulet, T. T. Luu, S. Pabst, R. Santra, Z. A. Alahmed, A. M. Azzeer, V. S. Yakovlev, V. Pervak, F. Krausz, and E. Goulielmakis, Science **334**, 195 (2011).
[4]A. Boguslavskiy, J. Mikosch, A. Gijsbertsen, M. Spanner, S. Patchkovskii, N. Gador, M. J. J. Vrakking, and A. Stolow, Science **335**, 1336 (2012).
[5]S. R. Leone, C. W. McCurdy, J. Burgdörfer, L. S. Cederbaum, Z. Chang, N. Dudovich, J. Feist, C. H. Greene, M. Ivanov, R. Kienberger, U. Keller, M. F. Kling, Z.-H. Loh, T. Pfeifer, A. N. Pfeiffer, R. Santra, K. Schafer, A. Stolow, U. Thumm, and M. J. J. Vrakking, Nat. Photonics **8**, 162 (2014).
[6]P. M. Kraus, B. Mignolet, D. Baykusheva, A. Rupenyan, L. Horny, E. F. Penka, G. Grassi, O. I. Tolstikhin, J. Schneider, F. Jensen, L. B. Madsen, A. D. Bandrauk, F. Remacle, and H. J. Woerner, Science **350**, 790 (2015).
[7]J. Breidbach and L. S. Cederbaum, Phys. Rev. Lett. **94**, 033901 (2005).
[8]B. Cooper and V. Averbukh, Phys. Rev. Lett. **111**, 083004 (2013).
[9]F. Calegari, D. Ayuso, A. Trabattoni, L. Belshaw, S. D. Camillis, S. Anumula, F. Frassetto, L. Poletto, A. Palacios, P. Decleva, J. B. Greenwood, F. Martin, and M. Nisoli, Science **346**, 336 (2014).
[10]M. Kling, C. Siedschlag, A. J. Verhoef, J. Khan, M. Schultze, T. Uphues, Y. Ni, M. Uiberacker, M. Drescher, F. Krausz *et al.*, Science **312**, 246 (2006).
[11]A. Cavalieri, N. Müller, and T. Uphues, Nature **449**, 1029 (2007).
[12]O. Smirnova, Y. Mairesse, S. Patchkovskii, N. Dudovich, D. Villeneuve, P. Corkum, and M. Y. Ivanov, Nature **460**, 972 (2009).
[13]S. Haessler, J. Caillat, W. Boutu, C. Giovanetti-Teixeira, T. Ruchon, T. Auguste, Z. Diveki, P. Breger, A. Maquet, B. Carre, R. Taieb, and P. Salières, Nat. Phys. **6**, 200 (2010).
[14]M. Krueger, M. Schenk, and P. Hommelhoff, Nature **475**, 78 (2011).
[15]J. D. Biggs, Y. Zhang, D. Healion, and S. Mukamel, Proc. Natl. Acad. Sci. U. S. A. **110**, 15597 (2013).
[16]D. Shafir, Y. Mairesse, D. Villeneuve, P. Corkum, and N. Dudovich, Nat. Phys. **5**, 412 (2009).
[17]P. Kraus, A. Rupenyan, and H. Wörner, Phys. Rev. Lett. **109**, 233903 (2012).
[18]J. Itatani, J. Levesque, D. Zeidler, H. Niikura, H. Pépin, J.-C. Kieffer, P. B. Corkum, and D. M. Villeneuve, Nature **432**, 867 (2004).
[19]A.-T. Le, R. Lucchese, S. Tonzani, T. Morishita, and C. Lin, Phys. Rev. A **80**, 013401 (2009).
[20]C. Lin, A.-T. Le, Z. Chen, T. Morishita, and R. Lucchese, J. Phys. B **43**, 122001 (2010).
[21]S.-I. Chu and V. I. Usachenko, Phys. Rev. A **71**, 063410 (2005).
[22]S. Patchkovskii, Z. Zhao, T. Brabec, and D. Villeneuve, Phys. Rev. Lett. **97**, 123003 (2006).
[23]M. Awasthi, Y. V. Vanne, A. Saenz, A. Castro, and P. Decleva, Phys. Rev. A **77**, 063403 (2008).
[24]L. Keldysh, Sov. Phys. JETP **20**, 1307 (1965).
[25]F. Faisal, J. Phys. B **6**, L312 (1973).
[26]H. R. Reiss, Phys. Rev. A **22**, 1786 (1980).
[27]J. Muth-Böhm, A. Becker, and F. Faisal, Phys. Rev. Lett. **85**, 2280 (2000).
[28]X. M. Tong, Z. X. Zhao, and C. D. Lin, Phys. Rev. A **66**, 033402 (2002).

[29]K. Mishima, M. Hayashi, J. Yi, S. Lin, H. Selzle, and E. Schlag, Phys. Rev. A **66**, 033401 (2002).
[30]A. Couairon and A. Mysyrowicz, Phys. Rep. **441**, 47 (2007).
[31]J. Kasparian, R. Sauerbrey, and S. Chin, Appl. Phys. B **71**, 877 (2000).
[32]A. Saenz, J. Phys. B **33**, 4365 (2000).
[33]X. Tong and C. Lin, J. Phys. B **38**, 2593 (2005).
[34]L. Nikolopoulos, T. K. Kjeldsen, and L. B. Madsen, Phys. Rev. A **76**, 033402 (2007).
[35]X. Chu, Phys. Rev. A **82**, 023407 (2010).
[36]S.-K. Son, S.-I. Chu *et al.*, Phys. Rev. A **80**, 011403 (2009).
[37]D. A. Telnov, S.-I. Chu *et al.*, Phys. Rev. A **79**, 041401 (2009).
[38]K. Yabana, T. Otobe, and J.-I. Iwata, *Progress in Ultrafast Intense Laser Science Volume I* (Springer, 2006), pp. 77–94.
[39]M. A. Marques and E. Gross, Annu. Rev. Phys. Chem. **55**, 427 (2004).
[40]X. Chu and M. McIntyre, Phys. Rev. A **83**, 013409 (2011).
[41]D. Bauer and F. Ceccherini, Opt. Express **8**, 377 (2001).
[42]R. Baer, D. Neuhauser, P. R. Ždánská, and N. Moiseyev, Phys. Rev. A **68**, 043406 (2003).
[43]X.-M. Tong and S.-I. Chu, Phys. Rev. A **64**, 013417 (2001).
[44]A. Crawford-Uranga, U. De Giovannini, E. Räsänen, M. J. T. de Oliveira, D. J. Mowbray, G. M. Nikolopoulos, E. T. Karamatskos, D. Markellos, P. Lambropoulos, S. Kurth *et al.*, Phys. Rev. A **90**, 033412 (2014).
[45]M. Hellgren, E. Räsänen, and E. K. U. Gross, Phys. Rev. A **88**, 013414 (2013).
[46]U. De Giovannini, D. Varsano, M. A. L. Marques, H. Appel, E. K. U. Gross, and A. Rubio, Phys. Rev. A **85**, 062515 (2012).
[47]P. Krause and H. B. Schlegel, J. Phys. Chem. Lett. **6**, 2140 (2015).
[48]P. Krause and H. B. Schlegel, J. Chem. Phys. **141**, 174104 (2014).
[49]C. M. Isborn and X. Li, J. Chem. Phys. **129**, 204107 (2008).
[50]S. A. Fischer, C. J. Cramer, and N. Govind, J. Chem. Theory Comput. **11**, 4294 (2015).
[51]J. I. Fuks, P. Elliott, A. Rubio, and N. T. Maitra, J. Phys. Chem. Lett. **4**, 735 (2013).
[52]J. I. Fuks, K. Luo, E. D. Sandoval, and N. T. Maitra, Phys. Rev. Lett. **114**, 183002 (2015).
[53]M. E. Casida, C. Jamorski, K. C. Casida, and D. R. Salahub, J. Chem. Phys. **108**, 4439 (1998).
[54]M. E. Casida and D. R. Salahub, J. Chem. Phys. **113**, 8918 (2000).
[55]N. T. Maitra, J. Chem. Phys. **125**, 014110 (2006).
[56]A. Dreuw, J. L. Weisman, and M. Head-Gordon, J. Chem. Phys. **119**, 2943 (2003).
[57]E. Livshits and R. Baer, J. Phys. Chem. A **110**, 8443 (2006).
[58]R. Baer and D. Neuhauser, Phys. Rev. Lett. **94**, 043002 (2005).
[59]M. Valiev, E. J. Bylaska, N. Govind, K. Kowalski, T. P. Straatsma, H. J. Van Dam, D. Wang, J. Nieplocha, E. Apra, T. L. Windus *et al.*, Comput. Phys. Commun. **181**, 1477 (2010).
[60]R. Krishnan, J. S. Binkley, R. Seeger, and J. A. Pople, J. Chem. Phys. **72**, 650 (1980).
[61]T. H. Dunning, J. Chem. Phys. **90**, 1007 (1989).
[62]P. Krause, J. A. Sonk, and H. B. Schlegel, J. Chem. Phys. **140**, 174113 (2014).
[63]J. P. Perdew and A. Zunger, Phys. Rev. B **23**, 5048 (1981).
[64]A. Dreuw and M. Head-Gordon, Chem. Rev. **105**, 4009 (2005).
[65]R. van Leeuwen and E. J. Baerends, Phys. Rev. A **49**, 2421 (1994).
[66]R. Baer, E. Livshits, and U. Salzner, Annu. Rev. Phys. Chem. **61**, 85 (2010).
[67]A. Potts and W. Price, in *Proceedings of the Royal Society of London A: Mathematical, Physical and Engineering Sciences* (The Royal Society, 1972), Vol. 326, pp. 181–197.
[68]E. Livshits and R. Baer, Phys. Chem. Chem. Phys. **9**, 2932 (2007).
[69]D. Chong, O. Gritsenko, E. Baerends *et al.*, J. Chem. Phys. **116**, 1760 (2002).
[70]T. Stein, L. Kronik, and R. Baer, J. Am. Chem. Soc. **131**, 2818 (2009).
[71]Y. Tawada, T. Tsuneda, S. Yanagisawa, T. Yanai, and K. Hirao, J. Chem. Phys. **120**, 8425 (2004).
[72]R. G. Fernando, M. C. Balhoff, and K. Lopata, J. Chem. Theory Comput. **11**, 646 (2015).
[73]S. Refaely-Abramson, S. Sharifzadeh, N. Govind, J. Autschbach, J. B. Neaton, R. Baer, and L. Kronik, Phys. Rev. Lett. **109**, 226405 (2012).
[74]T. Stein, L. Kronik, and R. Baer, J. Chem. Phys. **131**, 244119 (2009).
[75]A. Karolewski, L. Kronik, and S. Kümmel, J. Chem. Phys. **138**, 204115 (2013).
[76]K. Davies, H. Flocard, S. Krieger, and M. Weiss, Nucl. Phys. A **342**, 111 (1980).
[77]J. Theilhaber, Phys. Rev. B **46**, 12990 (1992).
[78]K. Yabana and G. F. Bertsch, Phys. Rev. B **54**, 4484 (1996).
[79]A. Castro, H. Appel, M. Oliveira, C. A. Rozzi, X. Andrade, F. Lorenzen, M. A. L. Marques, E. K. U. Gross, and A. Rubio, Phys. Status Solidi B **243**, 2465 (2006).
[80]X. Chu and S.-I. Chu, Phys. Rev. A **63**, 013414 (2000).
[81]K. B. Bravaya, D. Zuev, E. Epifanovsky, and A. I. Krylov, J. Chem. Phys. **138**, 124106 (2013).
[82]A. Szabo and N. S. Ostlund, *Modern Quantum Chemistry: Introduction to Advanced Electronic Structure Theory* (Courier Corporation, 2012).
[83]A. Castro, M. A. Marques, and A. Rubio, J. Chem. Phys. **121**, 3425 (2004).
[84]M. R. Provorse and C. M. Isborn, Int. J. Quantum Chem. **116**, 739 (2016).
[85]X. Li, S. M. Smith, A. N. Markevitch, D. A. Romanov, R. J. Levis, and H. B. Schlegel, Phys. Chem. Chem. Phys. **7**, 233 (2005).
[86]C.-L. Cheng, J. S. Evans, and T. Van Voorhis, Phys. Rev. B **74**, 155112 (2006).
[87]S. Meng and E. Kaxiras, J. Chem. Phys. **129**, 054110 (2008).
[88]W. Liang, C. T. Chapman, and X. Li, J. Chem. Phys. **134**, 184102 (2011).
[89]K. Lopata and N. Govind, J. Chem. Theory Comput. **7**, 1344 (2011).
[90]K. Lopata and N. Govind, J. Chem. Theory Comput. **9**, 4939 (2013).
[91]M. R. Hermann and J. Fleck, Jr., Phys. Rev. A **38**, 6000 (1988).
[92]J. L. Krause, K. J. Schafer, and K. C. Kulander, Phys. Rev. A **45**, 4998 (1992).
[93]J. S. Cohen, Phys. Rev. A **64**, 043412 (2001).
[94]T. K. Kjeldsen and L. B. Madsen, J. Phys. B **37**, 2033 (2004).
[95]V. P. Majety and A. Scrinzi, Phys. Rev. Lett. **115**, 103002 (2015).
[96]I. V. Litvinyuk, K. F. Lee, P. W. Dooley, D. M. Rayner, D. M. Villeneuve, and P. B. Corkum, Phys. Rev. Lett. **90**, 233003 (2003).
[97]D. Pavičić, K. F. Lee, D. M. Rayner, P. B. Corkum, and D. M. Villeneuve, Phys. Rev. Lett. **98**, 243001 (2007).
[98]B. Zhang and Z. Zhao, Phys. Rev. A **82**, 035401 (2010).
[99]Y. Liang, A. Talebpour, C. Chien, S. Augst, and S. Chin, J. Phys. B: At., Mol. Opt. Phys. **30**, 1369 (1997).
[100]X. Chu and S.-I. Chu, Phys. Rev. A **64**, 063404 (2001).
[101]S.-K. Son and S.-I. Chu, Chem. Phys. **366**, 91 (2009).
[102]K. A. Peterson, B. C. Shepler, D. Figgen, and H. Stoll, J. Phys. Chem. A **110**, 13877 (2006).
[103]M. Allan, E. Kloster-Jensen, and J. P. Maier, J. Chem. Soc., Faraday Trans. **73**, 1417 (1977).
[104]S. Tussupbayev, N. Govind, K. Lopata, and C. J. Cramer, J. Chem. Theory Comput. **11**, 1102 (2015).
[105]M. R. Provorse, B. F. Habenicht, and C. M. Isborn, J. Chem. Theory Comput. **11**, 4791 (2015).